# Multi-spectral Analysis of the Amazon Basin using SeaWinds, ERS, Seasat Scatterometers, TRMM-PR amd SSM/I

Haroon Stephen and David G. Long
Brigham Young University Microwave Earth Remote Sensing Laboratory
459 Clyde Building, Provo, UT 84602
TEL: 801-378-4884, FAX: 801-378-6586
e-mail: stephenh@ee.byu.edu and long@ee.byu.edu

***Abstract*** **– The Amazon basin represents a vast geographical zone containing large proportion of global biomass. We use the SeaWinds scatterometer (QSCAT), ERS-1/-2 scatterometer (ESCAT), NASA scatterometer (NSCAT), Seasat scatterometer (SASS), Tropical Rain Measuring Mission Precipitation Radar (TRMM- PR) and Special Sensor Microwave/Imager (SSM/I) data to study the multi-spectral microwave response of Amazon vegetation. Incidence angle signatures of combined backscatter measurements ($\sigma^o$) from the scatterometers and precipitation radar indicate a good inter-calibration of the sensors. The multi-frequency signatures of both $\sigma^o$ and radiometric temperature measurements ($T_b$) from SSM/I are also studied. Temporal variability of the Amazon basin is studied using C-band ERS data and a Ku-band time series formed by SASS, NSCAT and QSCAT data. ESCAT data reveals a possible mismatch in the calibration of scatterometers between ERS-1 and ERS-2. Although the central Amazon forest represents an area of very stable radar backscatter measurements, portions of the southern region exhibit backscatter changes over the past two decades.**

## I. Introduction

The spaceborne microwave remote sensing with its benefits of cloud penetration and sun independence provides a powerful tool to study extended areas like Amazon forest. Various land cover types of Amazon basin exhibit unique response in the different microwave bands [1,2]. We use SeaWinds scatterometer (QSCAT), ERS-1/-2 scatterometer (ESCAT), NASA scatterometer (NSCAT), Seasat scatterometer (SASS), Tropical Rain Measuring Mission (TRMM) Precipitation Radar (PR) and Special Sensor Microwave/Imager (SSM/I) to investigate multi-spectral signatures of Amazon forest. Some of the details of these sensors are summarized in Table I. Scatterometers and TRMM-PR (active) measure radar backscatter ($\sigma^o$) of the Earth's surface whereas the SSM/I is a seven channel radiometer (passive) which measures the surface radiometric temperature ($T_b$). $\sigma^o$ primarily depends upon the geometrical and dielectric properties of the target whereas $T_b$ is primarily a function of the emissivity and physical temperature of the target.

## II. Multi-spectral Signatures

The $\sigma^o$ response with incidence angle has been used extensively to distinguish different land cover types. A simple model is a straight line given by $\sigma^o = A + B(\theta - 40^o)$,

| Sensor | Incidence Angle | Years | Freq. (GHz) | Pol. | Res. (km) |
|---|---|---|---|---|---|
| SASS | 0°-70° | 78 | 14.4 | H V | 50 |
| ESCAT | 18°-59° | 91-00 | 5.3 | V | 50 |
| NSCAT | 17°-62° | 96-97 | 14.0 | H V | 50 |
| QSCAT | 46°& 54° | 99- | 13.4 | H V | 25 |
| TRMM-PR | 0°-17° | 97- | 13.8 | H | 4.4 |
| SSM/I-1 | 53° | 90- | 19.35 | H V | 69x43 |
| SSM/I-2 | 53° | 90- | 22.235 | V | 60x40 |
| SSM/I-3 | 53° | 90- | 37.0 | H V | 37x28 |
| SSM/I-4 | 53° | 90- | 85.5 | H V | 15x13 |

TABLE I
List of sensors used and their specifications

where $A$ (in dB) is the $\sigma^o$ at 40° incidence angle ($\theta$) and $B$ (in dB/°) is the slope of the line fit to the data. Figure 1 shows the $\sigma^o$ variation with $\theta$ from all the active instruments for three different land cover types. The data covers October of the year 1978, 1996 and 1999 for SASS, NSCAT and the remaining sensors, respectively. Comparison of the three plots confirms the previously known effects of surface and volume scattering over the three land cover types. The greater surface scattering from grasslands results in steeper $\sigma^o$ vs $\theta$ plots compared to the dense forest where it is predominantly volume scattering. The C-band $\sigma^o$ is lower than the Ku-band due to the larger wavelength of the C-band and hence greater penetration and greater losses. Moreover, the Ku-band wavelength is of the order of most plant-leaf-sizes resulting in greater volume scattering. The difference is more evident for near incidence angles and lower vegetation densities. These plots also reveal that C-band $\sigma^o$ vs $\theta$ has shallower slope than Ku-band and the offset between the two slopes reduces with the vegetation density. This is due to the difference in the penetration of the two bands which becomes more evident at greater vegetation densities. The increased moisture content of forest canopy and soil surface, from precipitation or flooding, further increases $\sigma^o$ and makes the slope of $\sigma^o$ vs $\theta$ plot shallower.

The three Ku-band sensors, although separated in time, provide a consistent behavior. The high variability of QSCAT data is predominantly noise caused by small foot print. The horizontal polarization (H-pol) $\sigma^o$ is generally higher than vertical polarization (V-pol).

The V-pol C-band and Ku-band $\sigma^o$ and V-pol $T_b$ from SSM/I are used to plot the frequency response of differ-

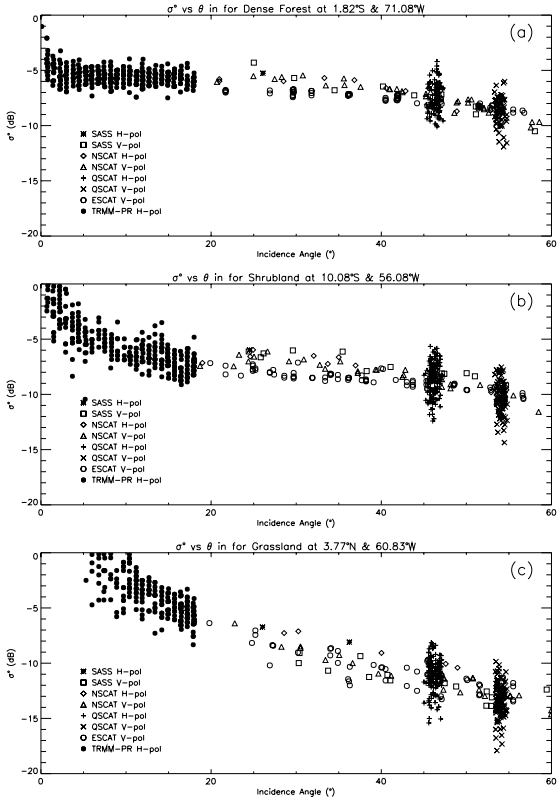


Fig. 1. Plots showing multi-spectral $\sigma^o$ variation with incidence angle using SASS, ESCAT, NSCAT, QSCAT and TRMM-PR data over selected (a) dense forest, (b) shrubland and (c) grassland.

ent land cover types as shown in Figure 2. The top plot is the response over the dense vegetation showing the data points and a line through the mean value at each frequency. The C-band and Ku-band data are normalized to 53° to make the incidence angle comparable to the SSM/I data. The active and passive channel regions are also indicated.

The $\sigma^o$ increases with frequency as seen in the last section, due to greater scattering at reduced wavelengths. The $T_b$ is expected to decrease with increase in frequency which is deviated at 85.5 GHz. The deviation results due to increased atmospheric emissions at higher frequencies which contaminate the signal at these frequencies. The bottom figure shows similar plots for different vegetation types, with only the line fit shown for clarity. The $T_b$ values at 85.5 GHz are discarded due to their atmospheric contamination. Different land cover types exhibit unique frequency responses. Both the $\sigma^o$ and $T_b$ lines lower with reduction in the vegetation density and a distinct inversion of slope for the first two SSM/I channels can be observed. This inversion from negative to positive slope occurs as the vegetation density reduces. The dense forest $T_b$ value is predominantly due to the emissions from forest canopy whereas over grassland, the soil emissions also contribute. The plot reveals that as the soil contribution

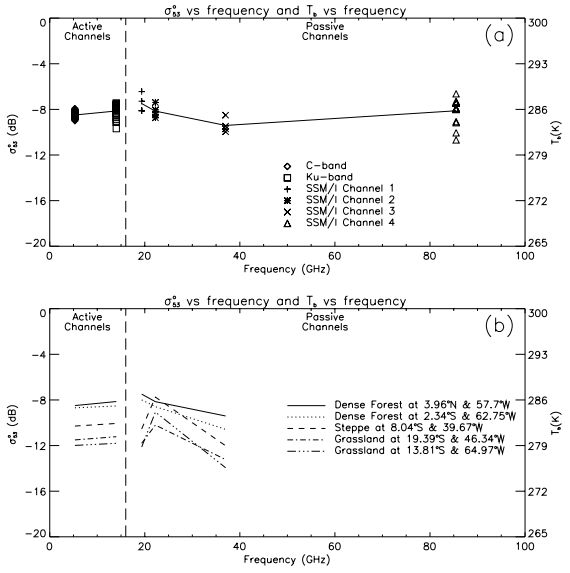


Fig. 2. Multi-spectral V-pol $\sigma^o$ and $T_b$ variation from scatterometers and radiometer, respectively over (a) dense forest and (b) different land cover types.

increases with a decrease in vegetation density, the emissions at 22.235 GHz become higher than at 19.5 GHz.

## III. Time Series

ESCAT and combined SASS, NSCAT and QSCAT data, provide a long C- and Ku-band $\sigma^o$ time series. Figure 3 (a) and (b) show time series plots of $A$ and $B$ from dense forest and its boundary, respectively. The $A$ and $B$ values are calculated using the linear equation mentioned in Section II where the normalization is made to 54° incidence angle to match with QSCAT data. The normalized $A$ values do not exactly match the QSCAT $A$ measurements, due to a bias from approximating $\sigma^o$ vs $\theta$ by a straight line. The bias is minimum at mid-incidence angles and increases at near and far ranges.

The $A$ time series from the dense forest (a) has a very stable backscatter for both the frequencies during the last two decades. The $B$ plot is noisier and has a positive step in the C-band during 1996. The ESCAT was switched from ERS-1 to ERS-2 in this year. Since Ku-band does not show any significant change in the mean $B$ value between 1978 and 1996, the step in the ESCAT data is probably attributed to calibration differences of the two ERS scatterometers. The $B$ plot from forest boundary (b) also shows similar step but is less evident due to seasonal variations. This latter plot corresponds to an area suspected to have undergone deforestation. The C-band $A$ plot reveals a gradual increase in the amplitude of the seasonal fluctuation over the decade whereas the yearly mean of $A$ is found to decay with time. This effect is more significant after 1996 and can also be seen in the Ku-band data. Although this could be due to the ESCAT data quality, a

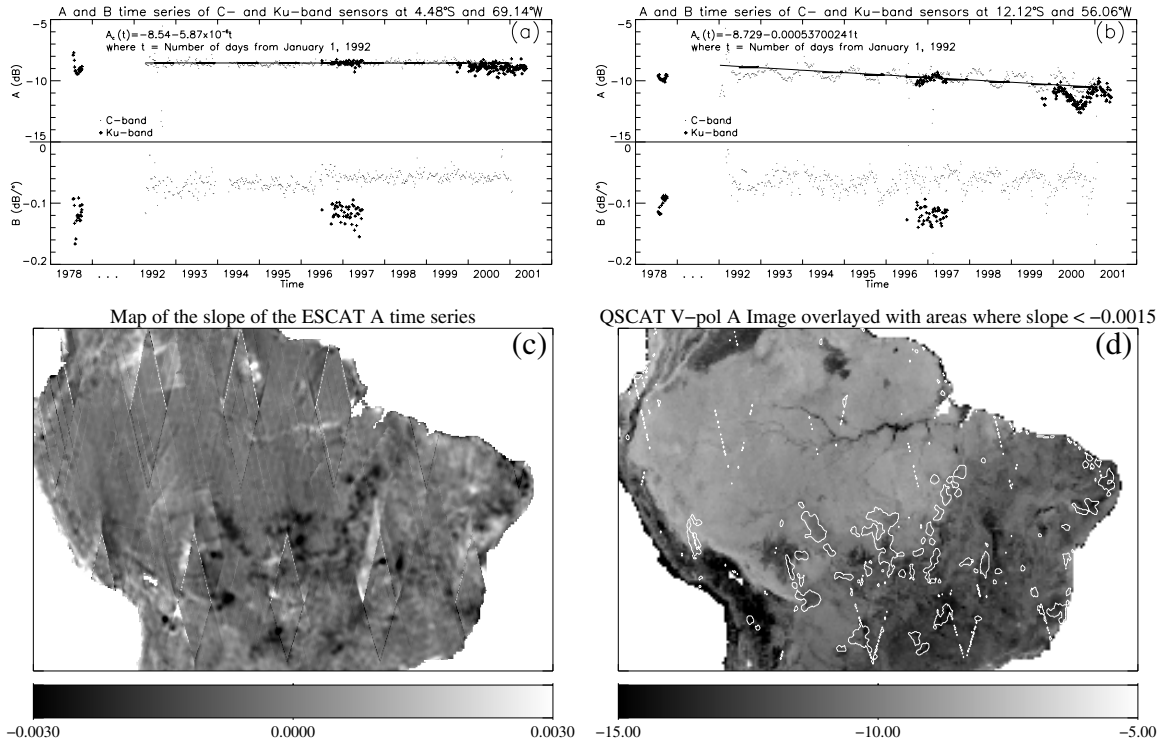


Fig. 3. Time Series of $A$ and $B$ values from C- and Ku-band data over the (a) dense forest and (b) fringes of the dense forest. (c) shows the slope the ESCAT $A$ decade long time series over Amazon basin and (d) is QSCAT V-pol image. The overlaid contours correspond to the areas where ESCAT time series slope is less than -0.0015

similar trend at Ku-band suggests that the primary cause is geophysical variation, possibly a reduction in canopy density. The solid line is a fit to the ESCAT time series and its equation is also shown. The line has a slope of -0.0005 dB/day with a decrease of about 1.8 dB in the mean $A$ over eight years. Similar trend is observed at many other locations on forest boundary. The time series of ESCAT $A$ over the whole Amazon basin is fit with a straight line. Figure 3(c) is the map of the slope of the line fit at each pixel. The diamond shaped artifacts are the noise from using multiple swaths. The slope value in the dense forest area is close to zero confirming its temporal stability. In the southern region, dark patches have low slope values and indicate areas where the decrease in $A$ is significant. This must be related to geophysical changes in the area such as reduced moisture and/or vegetation density. The location of these areas at the fringes of the forest suggests that they are possibly the areas of reduced canopy cover. Most of these areas are found to have slope smaller than -0.0015 dB/day. The slope map is thresholded at this value and overlaid onto the QSCAT V-pol $A$ image shown in 3(d). The overlaid patches are the areas of possible deforestation. There are a few areas of positive slope, possibly due to increasing vegetation density.

## IV. Conclusion

A simple multi-spectral analysis of the Amazon basin is conducted. The scatterometers and TRMM-PR $\sigma^o$ variations with incidence angle show distinctive behavior for different vegetation densities. The different sensors are well inter-calibrated. Different land cover types are found to exhibit unique frequency responses of $\sigma^o$ and $T_b$. The C- and Ku-band time series reveal a small calibration mismatch between ESCATs aboard ERS-1 and ERS-2 satellites. A gradual decrease in ESCAT $A$ fit with a straight line and its slope used to identify areas of significant $A$ reduction possibly caused by geophysical changes. Low-slope regions are found, mostly at the Southern boundary of the Amazon forest, which could be due to deforestation.

## References

[1] D. G. Long and P. J. Hardin, "Vegetation studies of the Amazon basin using enhanced resolution Seasat scatterometer data," *IEEE Trans. Geosci. Rem. Sens.*, vol. 32, pp. 449–460, March 1994.

[2] G. Macelloni, S. Paloscia, P. Pampaloni, and R. Ruisi, "Airborne multifrequency L- to Ka band radiometric measurements over forests," *IEEE Trans. Geosci. Rem. Sens.*, vol. 39, pp. 2507–2513, November 2001.